

$K\alpha$ hypersatellite lines of medium-mass atoms induced by 100-MeV ${}^4\text{He}^{2+}$ ions

B. Boschung, J.-Cl. Dousse, B. Galley, Ch. Herren, J. Hozzowska, J. Kern, and Ch. Rhème
Physics Department, University of Fribourg, CH-1700 Fribourg, Switzerland

Z. Halabuka
Physics Department, University of Basel, CH-4056 Basel, Switzerland

T. Ludziejewski, P. Rymuza, and Z. Sujkowski
Institute for Nuclear Studies, 05-400 Swierk, Poland

M. Polasik
Faculty of Chemistry, Nicolas Copernicus University, 87-100 Torun, Poland
 (Received 12 September 1994)

The radiative decay of double K -shell vacancies in zirconium ($Z = 40$), molybdenum ($Z = 42$), and palladium ($Z = 46$) was observed using a high-resolution transmission crystal spectrometer. The samples were ionized by the impact of 100-MeV ${}^4\text{He}^{2+}$ ions. From the well resolved $K^{-2} \rightarrow K^{-1}L^{-1}$ transitions, the energies, linewidths, intensity ratios, and double K -shell ionization cross sections were deduced. The experimental energies and linewidths of the hypersatellites are compared with results of Dirac-Hartree-Slater calculations and with multiconfiguration-Dirac-Fock calculations, both taking into account the Breit interaction. For the extracted double K -shell ionization cross sections a comparison is made with the semiclassical approximation predictions within the independent-particle model.

PACS number(s): 32.30.Rj, 32.70.Jz, 32.70.Fw, 32.80.Hd

I. INTRODUCTION

The construction of facilities allowing one to accelerate almost all types of projectiles in a wide range of energies has opened during the last decades a wide field of investigation. In particular, special interest has risen for experiments involving multiply ionized atoms, leading to a better understanding of the collision and ionization processes and of the decay modes of ionized atoms.

Ionized atoms may decay by emission of x rays or by nonradiative processes, such as Auger or Coster-Kronig transitions. Nonradiative decay is predominant for light elements, whereas heavy atoms decay mainly by emission of x rays. X rays produced by the radiative decay of singly ionized atoms are called diagram lines. Compared to singly ionized atoms, the electronic screening of the nuclear charge is weaker in multiply ionized atoms, resulting in an increase of the binding energy of the remaining electrons. In such atoms radiative transitions are, therefore, shifted toward higher energies with respect to the corresponding diagram lines and give rise to so-called satellite x-ray lines. In general, the energy shifts of these satellite transitions increase with the principal quantum number characterizing the electron undergoing the transition and decrease with the principal quantum number of the spectator vacancy. For molybdenum, shifts of about 48 eV for the first $K\alpha L^1$ satellite [1] and about 14 eV for the first $K\beta_{1,3}M^1$ satellite [2] were observed. The energy shift is the most pronounced in the case where the innermost shell is empty. $K^{-2} \rightarrow K^{-1}X^{-1}$ transitions are named hypersatellites. For mid- Z atoms, the $K\alpha$ hypersatel-

lite lines ($K^{-2} \rightarrow K^{-1}L^{-1}$) are expected to be shifted by about 400–500 eV with respect to the corresponding diagram lines.

Different processes can lead to double K vacancies. The latter may occur in atoms during nuclear decay as a result of K -shell internal conversion or β decay [3–5]. In this case the second K electron is ejected by a shake-off process. Only small double ionization cross sections are achieved by these processes, leading to long-winded and difficult experiments. Similar problems are encountered when the vacancies are produced by photoionization [6,7] or electron bombardment [8,9].

Significantly higher cross sections are obtained in collisions with heavy ions [10–13], but in this case, the probability of additional ionization in outer shells is no more negligible, resulting in complex x-ray spectra from which it is very difficult to resolve properly the hypersatellites.

Nevertheless, between these two extremes one may find conditions where a satisfactory double ionization cross section is achieved and the probability for simultaneous ionization in outer shells is negligible. For medium-mass target atoms, such favorable conditions are met with light ions of 20–25 MeV/amu. At these energies the double K -shell ionization cross sections are close to their maximum values, whereas the L - and M -shell ionization probabilities are on the contrary markedly smaller than their largest values, which are found at 2–3 times lower projectile velocities (see Fig. 1).

K hypersatellites are in several respects very useful for studying atomic systems. A precise measurement of their energies constitutes a sensitive test of the contribution of the Breit interaction to the Coulomb potential. Natu-

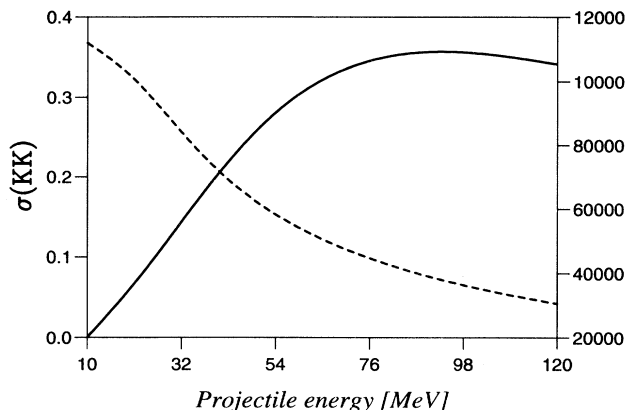


FIG. 1. Molybdenum double K -shell ionization cross section $\sigma(KK)$ and single L -shell ionization cross section $\sigma(L)$ in barns versus ${}^4\text{He}^{2+}$ projectile energy. The calculations were performed with the SCA independent-particle model. The solid line represents the double K -shell ionization cross section $\sigma(KK)$, the dashed line the single L -shell ionization cross section $\sigma(L)$.

ral linewidths of K hypersatellites, which are expected to be 2–3 times larger than those of the corresponding diagram lines, allow one to deduce the widths of double K -hole excited states. Interesting conclusions concerning the coupling scheme applicable to the investigated target atoms can be drawn from the $K\alpha_1$ to $K\alpha_2$ hypersatellite yield ratios. Multiple ionization induced in atoms by collisions with charged projectiles is generally assumed to result from the sum of uncorrelated single ionization processes. The validity of this hypothesis can be checked by comparing the measured cross sections σ_{KK} of double K -shell ionization with theoretical predictions as those given for instance by the independent particle semiclassical approximation model (SCA).

In spite of the above mentioned interesting characteristics of K hypersatellites, available experimental information is scarce and concerns mainly light atoms. For heavier atoms, most of the measurements were performed by means of the coincidence method in which the x rays emitted by the cascade $K^{-2} \rightarrow K^{-1}L^{-1}$ ($K\alpha$ hypersatellites) $K^{-1}L^{-1} \rightarrow L^{-2}$ ($K\alpha L$ satellites) are detected in coincidence by two semiconductor detectors [5]. In these experiments, however, due to the restricted resolution of the detectors, no hypersatellite natural linewidths can be determined.

In this paper we present results on the energies, linewidths and relative intensities of $K\alpha_1$ and $K\alpha_2$ hypersatellites induced in metallic targets of zirconium ($Z = 40$), molybdenum ($Z = 42$) and palladium ($Z = 46$) by the impact of 100 MeV ${}^4\text{He}^{2+}$ ions. The measurements were performed by high-resolution crystal diffraction. From the measured hypersatellite yields, the double K -shell ionization cross sections were also deduced and compared to SCA predictions.

II. EXPERIMENT

The experiments were performed at the Paul Scherrer Institute in Villigen, Switzerland. The ${}^4\text{He}$ ions were accelerated to 100 MeV by the variable energy Philips Cyclotron and focused to a 1 mm wide and 20 mm high beam spot corresponding to the dimensions of the targets. The experiments were carried out with ${}^4\text{He}^{2+}$ beam currents of 3 μA for Zr and Mo and 1.8 μA for Pd.

Self-supporting metallic targets of natural zirconium, molybdenum, and palladium with thicknesses of 12.7 mg/cm², 26.4 mg/cm², and 25.9 mg/cm², respectively, were used. The targets were cooled by a low pressure He gas flowing through the target chamber. The latter was isolated from the high vacuum beam pipe by two 5.3 mg/cm² thick havar foils.

The x rays from the target were measured with an on-line transmission crystal spectrometer [14] in modified DuMond slit geometry. In this geometry a 0.15-mm-wide slit, placed on the focal circle between the target and the crystal, acts as the effective source of radiation (see Fig. 2). With respect to the standard DuMond geometry (no slit and target thickness perpendicular to the direction of observation), this setup allowed us to obtain higher luminosity and to cancel phenomena like thermal deformation of the target, affecting the profile of the observed lines. The 0.15-mm aperture of the slit was chosen as a compromise between two effects influencing, respectively, the intensity and the width of the observed x rays: the luminosity of the spectrometer, which has to be as

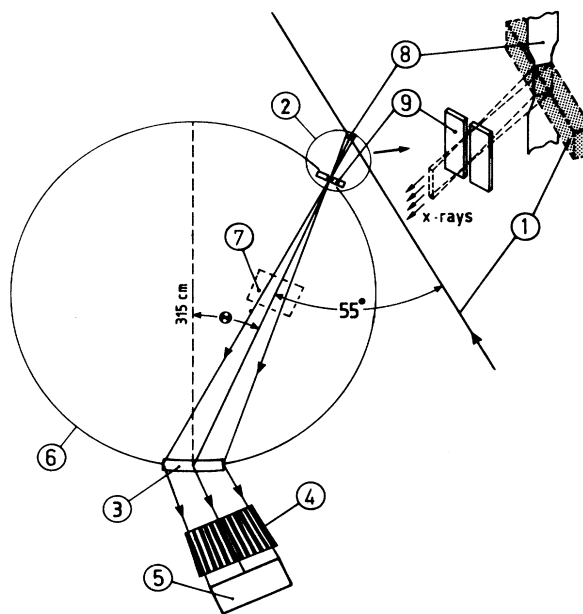


FIG. 2. Schematic diagram of the DuMond slit geometry used in this experiment (not to scale): (1) beam, (2) target chamber, (3) crystal, (4) collimator, (5) detector, (6) focal circle, (7) monitor detector, (8) target, and (9) tantalum slit. Θ represents the Bragg angle.

high as possible, and the instrumental resolution that depends mainly in this geometry on the slit width. More details about this geometry can be found in Ref. [15].

The spectrometer was operated by a 68000-based multitask modular computer system via standard VME and EUROBUS electronic modules. An efficient and versatile user program package was developed by the author [16]. This package, written in C, controlled all aspects of the measurements. Peripherals allowing on-line visualization of the data were attached. The acquisition electronics was connected to the computer through a 4096 channels dead-time corrected analog-to-digital converter (ADC). A preliminary sorting of the ADC data was performed on line in order to reject unwanted and nonprompt energy events. The steering modules controlling the laser interferometer, the step-motors of the spectrometer and the target chamber were supervised by a Z80 microcomputer and enclosed in a EUROBUS crate. The latter and the analogical electronics of the detectors were located in the experimental area close to the spectrometer, while the computer system and the ADC were placed in a separate room at a distance of about 60 m. The digital signals were transferred between the experimental area and the computer room via optical fibers.

The (110) reflecting planes of a 1-mm-thick natural quartz crystal plate were used for the diffraction of the x rays. The curvature radius of the crystal was 3.15 m and the reflecting area $5 \times 5 \text{ cm}^2$. The 25.651 50(7) keV γ decay of an intense ^{161}Tb calibration source [17] was used to determine the instrumental response induced mainly by the slit aperture and the imperfect crystal curvature. Including the contribution of the slit (~ 9.9 arcsec) the total instrumental response was found to be a Gaussian with a full width at half maximum of 11.2 ± 0.2 arcsec. The reflection angles were measured by means of an optical laser interferometer, which has been described in details in Ref. [14].

The diffracted x rays were detected by a 1-mm-thick NaI scintillation detector, surrounded by an anti-Compton ring. We have taken advantage from the time structure of the beam (20-ns bursts with a repetition rate of 10 MHz) to reduce the beam uncorrelated background by performing coincidences between the events from the spectrometer central detector and the rf signal of the cyclotron.

The beam intensity was monitored by a 0.4-cm^3 Si(Li) detector placed in front of the spectrometer, below the target-crystal axis, and viewing the target through the same slit as the crystal. In the Si(Li) energy spectrum, selected regions corresponding to the $K\alpha$ and $K\beta$ x rays of interest were chosen for each target. The integrated numbers of events pertaining to the selected regions were then used to control the data acquisition of the spectrometer performed in the preset count mode. All points of a given crystal spectrometer spectrum correspond, therefore, to equal numbers of projectile-target collisions.

The energy calibration of the spectra was based on the $K\alpha_1$ diagram lines measured on both sides of reflection. The energies of these transitions were taken from the compilation of experimental values of Bearden and Burr [18].

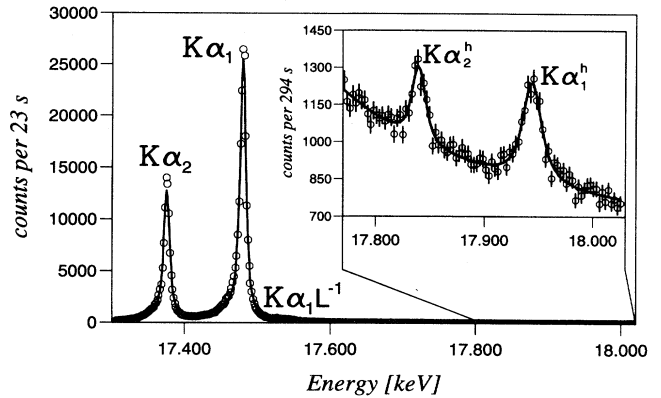


FIG. 3. Crystal spectrometer $K\alpha$ x-ray spectrum of molybdenum induced by 100 MeV $^4\text{He}^{2+}$ ions. The result of a single hypersatellite region scan is represented in the inset. On the high-energy tail of the $K\alpha_1$ line, one can distinguish the weak $K\alpha_1 L^{-1}$ satellite.

All spectra were collected in first order on the right side of reflection by step scanning over the desired angular region. In order to survey the stability and the reproducibility of the experimental setup, which is of particular importance for such time consuming measurements, the hypersatellites were measured in several successive scans. Moreover, a control measurement of the $K\alpha_1$ diagram line was performed between each scan. The crystal spectrometer $K\alpha$ x-ray spectrum of molybdenum is shown for illustration in Fig. 3.

III. DATA ANALYSIS

The profile of an x-ray line measured with a crystal spectrometer can generally be represented by the convolution of a Lorentzian and a Gaussian. The latter corresponds to the instrumental response of the spectrometer and the Lorentzian represents the natural line shape of the x-ray transition. The convolution of these two lines results in a so-called Voigt profile.

The observed spectral lines were analyzed by means of a least-squares-fitting program (program package MINUIT from CERN library PACKLIB [19]) employing such Voigt functions. Except for zirconium (see below), all diagram and hypersatellite lines were fitted with single Voigt-profiles. The beam uncorrelated background was taken into account by adding a constant value to the fitting function.

The width of the Gaussian instrumental response was extracted from the measurement of the Tb 25.652-keV γ decay. For all spectra, the energies and the intensities of the transitions, as well as the widths of the Lorentzian profiles were let free. In this way the correlations between the different free parameters were considered in the error estimation of the fitting procedure.

As the weak hypersatellite transitions were laying on

TABLE I. Correction factors of the observed transition intensities for the self-absorption in the target and the intensity attenuation in the crystal. The factors were normalized to give 1.000 for the $K\alpha_1$ diagram transitions.

Element	Intensity correction factors		
	$K\alpha_2$	$K\alpha_1^h$	$K\alpha_2^h$
^{40}Zr	1.029	0.868	0.890
^{42}Mo	1.031	0.879	0.904
^{46}Pd	1.027	0.920	0.942

the high-energy tails of the much stronger diagram lines, the spectra were analyzed in the following way. First, the $K\alpha_1$ and $K\alpha_2$ diagram lines were fitted. The obtained values for the energies and the natural linewidths of the diagram lines were then used to fit the background structure of the hypersatellite spectra. As the time scale was different for the two spectra, the intensity of the $K\alpha_1$ line was let free, whereas the $K\alpha_2$ to $K\alpha_1$ yield ratio was kept constant. A very good agreement with the observed background of the hypersatellite spectra could be obtained thereby. The two conspicuous hypersatellite transitions were then analyzed using again Voigt profiles with energies, intensities, and Lorentzian widths as free parameters. This method gave the most reliable results. Finally, yields obtained from the fitting procedure were corrected for the self-absorption of the observed x rays in the target and their intensity attenuation by the crystal thickness. The corresponding correction factors are given in Table I. Corrections concerning the dependence on the energy of the crystal reflectivity were estimated to be smaller than 1% and, therefore, not considered.

In K -shell ionizing collisions of heavy ions with atoms, the additional multiple M -shell ionization produces a broadening and an energy shift of the x-ray lines [20]. It is

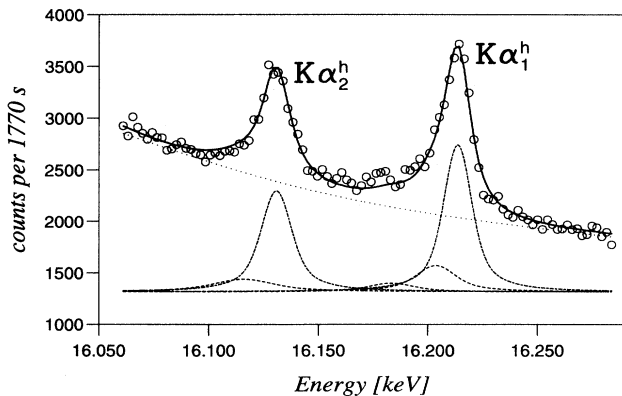


FIG. 4. $K\alpha$ hypersatellite spectrum of zirconium induced by 100 MeV $^4\text{He}^{2+}$ ions. The thick solid line corresponds to the total fit of the spectrum, the dotted one to the sum of the tails of the Voigt profiles used to fit the diagram transitions, background included. Fitted profiles of the hypersatellites and of the additional lines used to take into account the observed low-energy asymmetries (see text) are also represented.

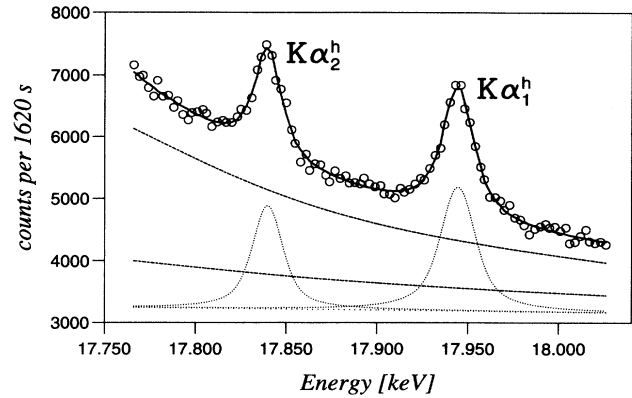


FIG. 5. $K\alpha$ hypersatellite spectrum of molybdenum induced by 100 MeV $^4\text{He}^{2+}$ ions. The thick solid line corresponds to the total fit of the spectrum. $K\alpha_1$ and $K\alpha_2$ tails as well as fitted profiles of hypersatellites are represented.

well known that the importance of these effects increases with the squared charge of the projectile. Furthermore, the broadening of the lines and their shifts in energy are the largest when the projectile velocity matches the velocity of the M -shell electrons of the target atom. Since in our experiment we have used light projectiles and a beam energy far above to energy corresponding to the mentioned matching velocity condition, the additional M -shell ionization can be neglected and was, therefore, not taken into account in the data analysis.

Problems were encountered during the analysis of the zirconium data. Indeed, the $K\alpha_1$ and $K\alpha_2$ diagram transitions, as well as the corresponding hypersatellite lines showed obvious asymmetries on their low-energy tails (see e.g., Fig. 4).

Similar low-energy structures were observed by various authors in the K x-ray emission spectra of metals. Different explanations were proposed. For light elements, the asymmetries were attributed to plasmon excitation during x-ray emission. Such plasmons were observed for instance in the $K\alpha$ emission of beryllium [21] and graphite

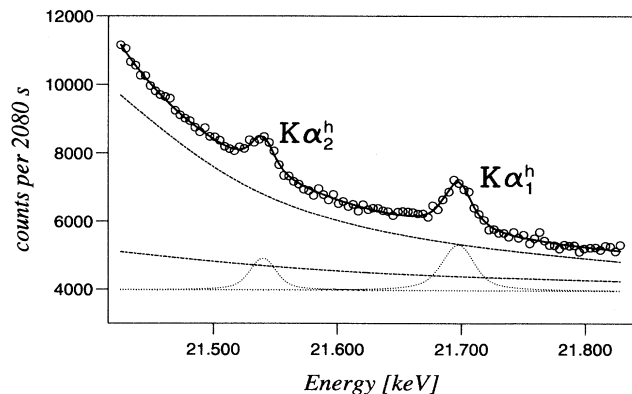


FIG. 6. Same as Fig. 5 but for palladium.

[22]. For transition metals, the low-energy asymmetries were suggested to be due to the interaction between the electrons of the incomplete $3d$ or $4d$ subshell and those of the unfilled inner shell owing to the emission of the measured x rays [23].

In the fitting procedure additional Voigt profiles, two for the $K\alpha_1$ transition and one for the $K\alpha_2$, were used to account for the observed asymmetries. The energies, Lorentzian widths, and relative intensities of the additional lines were let free in the analysis of the $K\alpha$ diagram transitions. The obtained values were then used as fixed parameters in the analysis of the hypersatellite spectrum.

The observed and fitted $K\alpha$ hypersatellite spectra of zirconium, molybdenum, and palladium are represented in Figs. 4, 5, and 6, respectively.

IV. RESULTS AND DISCUSSION

A. Energies

The energies of the main diagram lines have been measured with high precision since a long time, whereas those of the hypersatellites are not very well known. It was shown by Chen *et al.* [24] that the Breit interaction, i.e., the interaction between any two atomic electrons due to the exchange of a single transverse photon, affects the multiplet splitting of double vacancy configurations in atoms. This influences the transition energies as well as the transition probabilities. For medium-mass atoms, the relative contribution of the Breit interaction to the energy shifts of $K\alpha_1$ hypersatellites was estimated by Chen to be about 5–6%, i.e., ~ 25 eV for Zr, ~ 26 eV for Mo, and ~ 29 eV for Pd. In these calculations Dirac-Hartree-Slater (DHS) wave functions were used. For comparison multiconfiguration Dirac-Fock (MCDF) calculations with the GRASP computer code [25,26] including also the Breit interaction and QED (self-energy and vacuum polarization) corrections, and using Dirac-Fock wave functions were performed. The transition energies as well as the intensity ratios were calculated using the modified special average level version of the MCDF method [27].

The measured energy shifts of the hypersatellite transitions with respect to the parent diagram lines are given in Table II, where they are compared to the results of

TABLE II. Measured energy shifts in eV of $K\alpha_{1,2}$ hypersatellites with respect to the parent diagram lines compared to calculations using the MCDF method. Theoretical predictions based on DHS calculations of Chen are also given for comparison, whereby the values for Mo and Pd are interpolated.

Element	Energy shifts in eV					
	$E(K\alpha_1^h) - E(K\alpha_1)$			$E(K\alpha_2^h) - E(K\alpha_2)$		
	expt.	MCDF	DHS	expt.	MCDF	DHS
$_{40}\text{Zr}$	438.1(1.0)	438.5	438.9	438.9(1.0)	438.4	439.1
$_{42}\text{Mo}$	465.2(1.0)	463.7	466.0	465.4(1.0)	464.3	466.0
$_{46}\text{Pd}$	520.1(1.3)	520.5	520.8	519.8(1.9)	519.7	520.4

MCDF and DHS calculations. For Mo and Pd the DHS values were obtained by interpolation.

Quoted errors are purely statistical and correspond to 1 σ standard deviation. Excellent agreement is found with the theoretical predictions confirming the Breit contribution to the transition energies of the $K\alpha^h$ hypersatellites.

B. Natural linewidths

Due to the double vacancy state in the K shell, the natural linewidths of the hypersatellites are expected to be much larger than the ones of the corresponding diagram lines. In fact, the width of an x-ray transition is theoretically equal to the sum of the total widths of the initial and final states. In the case of doubly ionized atoms, the width of the initial state (K^{-2}), with two vacancies in the K shell, can be estimated to be twice the width of a single K vacancy level, i.e., $2\Gamma_K$. In the same manner, the width of the final state ($K^{-1}L^{-1}$) is approximated by $\Gamma_K + \Gamma_L$. The natural widths of the hypersatellites should thus be equal to $3\Gamma_K + \Gamma_L$ [28]. We compare in Table III the natural linewidths obtained in our experiment with the values calculated with this phenomenological law. The single vacancy level widths were taken from Krause and Oliver [29], where effects influencing the broadening of the level widths (like multiple ionization, etc.) are not taken into account. A quite satisfactory agreement is found between theory and experiment. This statement however has to be appreciated cautiously, since the level widths of Krause are given with quite large uncertainties (4% for the K level and up to 20% for the L levels) and because only statistical errors are quoted for the experimental results.

C. $K\alpha_1^h/K\alpha_2^h$ yield ratios

Whereas for diagram transitions the $I(K\alpha_1)/I(K\alpha_2)$ intensity ratios are close to two and their variation with the atomic number Z is small, the hypersatellite $I(K\alpha_1^h)/I(K\alpha_2^h)$ yield ratios are subject to strong variations [30]. Indeed, considering light atoms where the LS coupling is dominant, the $K\alpha_1^h$ spin-flip transition ($^1S_0 \rightarrow ^3P_1$) is forbidden. For that reason, this transition is strongly delayed for light atoms and the rela-

TABLE III. Natural linewidths in eV of $K^{-2} \rightarrow K^{-1}L^{-1}$ transitions. The calculated values were obtained with the phenomenological law proposed by Mossé *et al.* [28] using semiempirical single vacancy level widths from [29].

Element	$K\alpha_1^h$		$K\alpha_2^h$	
	expt.	calc.	expt.	calc.
$_{40}\text{Zr}$	11.7(1.3)	13.1(6)	13.2(2.2)	13.3(6)
$_{42}\text{Mo}$	19.5(2.1)	15.3(6)	16.6(2.4)	15.5(7)
$_{46}\text{Pd}$	24.1(4.4)	21.0(9)	19.5(5.9)	21.2(9)

TABLE IV. Comparison of hypersatellite intensity ratios $I(K\alpha_1^h)/I(K\alpha_2^h)$ between our experimental results, calculations using MCDF method and calculations done by Chen *et al.* [24] using DHS wave functions, both including Breit interaction. With the exception of Zr, the theoretical intensity ratios of Chen are interpolated.

Element	Intensity ratio $I(K\alpha_1^h)/I(K\alpha_2^h)$		
	expt.	MCDF	DHS
^{40}Zr	1.38(23)	1.04	1.04
^{42}Mo	1.34(19)	1.14	1.13
^{46}Pd	1.71(45)	1.31	1.31

tive yields $I(K\alpha_1^h)/I(K\alpha_2^h)$ are nearly zero. In heavy atoms, where the jj coupling is predominant, the $K\alpha_1^h$ transitions are no longer hindered and the intensity ratios $I(K\alpha_1^h)/I(K\alpha_2^h)$ tend to two as in the case of the diagram transitions. $I(K\alpha_1^h)/I(K\alpha_2^h)$ yield ratios of medium-mass atoms, which are expected to increase with the atomic number Z between these two extreme values, represent thus a sensitive tool to check the intermediate coupling model.

The $I(K\alpha_1^h)/I(K\alpha_2^h)$ intensity ratios extracted from our measurements are listed in Table IV, where they are compared to theoretical predictions. The intensity corrections presented in Sec. III are included in the experimental values. The increase of relative uncertainties with increasing atomic numbers is due mainly to the peak-to-background ratio of the hypersatellites which decreases with Z (see Figs. 4, 5, and 6).

An overview of the experimental $I(K\alpha_1^h)/I(K\alpha_2^h)$ yield ratios obtained by different authors for elements ranging from Ti ($Z = 22$) to Pb ($Z = 82$) is given in Fig. 7. Most of the experimental values are in satisfactory agreement with the DHS predictions of Chen *et al.* [24].

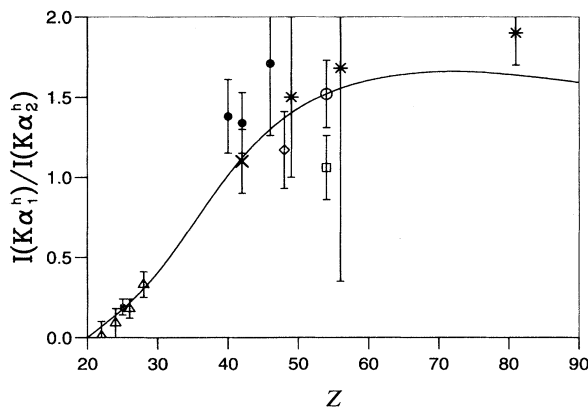


FIG. 7. $K\alpha_1^h$ to $K\alpha_2^h$ hypersatellite intensity ratios as a function of the atomic number Z . The solid line represents the results of DHS calculations by Chen *et al.* [24]. The symbols correspond to experimental values: \triangle Ref. [7], \square Ref. [48], \circ Ref. [49], \blacksquare Ref. [50], \diamond Ref. [51], \times Ref. [52], $*$ Ref. [31,32], \bullet this work.

Our results seem to be systematically larger than the theoretical predictions by 20–30%. A less pronounced but similar tendency can be observed in the results obtained by Briand *et al.* [31,32]. However, no definitive conclusion can be drawn, the relative uncertainties being of the same order of magnitude or larger than the observed differences.

D. Double K -shell ionization cross sections

Double K -shell ionization cross sections can be deduced from absolute yields of K hypersatellites. Absolute intensity measurements are, however, difficult to carry out by crystal diffractometry because parameters that are not known very well, like for instance the solid angle of the spectrometer or the reflectivity of the crystal, are needed. Relative intensities, on the contrary, can be measured with high precision provided that the energies of the compared transitions are not too different. For this reason, we have determined first the cross section ratios σ_{KK}/σ_K with the method described below. Using the fact that experimental cross sections for single K -shell ionization by light ions are very well reproduced by SCA calculations, we deduced then the cross sections σ_{KK} by means of the following relation:

$$\sigma_{KK}^{\text{expt}} = \left(\frac{\sigma_{KK}}{\sigma_K} \right)_{\text{expt}} \sigma_K^{\text{SCA}}. \quad (1)$$

The double to single ionization cross section ratio can be expressed as

$$\frac{\sigma_{KK}}{\sigma_K} = \frac{\omega_K}{\omega_{KK}} \frac{\sum I(K^{-2} \rightarrow K^{-1}X^{-1})}{\sum I(K^{-1} \rightarrow X^{-1})}, \quad (2)$$

where ω_{KK} and ω_K are the fluorescence yields of the doubly and singly, respectively, K -shell ionized atoms, I stands for the intensity of the radiative transitions and X represents every possible subshell.

Available experimental and theoretical information about fluorescence yields of doubly K shell ionized atoms is rare. The single data that we could find in the literature are results of calculations performed by Bhalla for neon [33,34]. Strong differences in the fluorescence yields are predicted by these calculations, depending whether the Ne atom is purely doubly ionized in the K shell or multiply ionized. For pure doubly K -shell ionized atoms the fluorescence yields are nearly equal to those of singly ionized atoms, whereas for multiply ionized atoms with empty K -shell and additional holes in the L -shell values up to two times larger are obtained.

If we assume that in a $K^{-2}L^{-n}$ multiple ionization the K - and L -shell electrons are ejected independently, the cross section for producing such a highly excited state is given by the binomial distribution

$$\sigma(K^{-2}L^{-n}) = \int_0^{+\infty} p_K^2(b) \binom{8}{n} p_L^n(b) [1 - p_L(b)]^{8-n} \times 2\pi b db, \quad (3)$$

where b is the impact parameter and p_K and p_L are the

TABLE V. MCDF theoretical intensity ratios.

Element	$I(K\beta)/I(K\alpha)$	$I(K\beta^h)/I(K\alpha^h)$
${}_{40}\text{Zr}$	0.185	0.189
${}_{42}\text{Mo}$	0.191	0.199
${}_{46}\text{Pd}$	0.202	0.205

K - and L -shell ionization probabilities per electron. Further, since p_L is nearly constant in the impact parameter range where p_K is not vanishing, Eq. (3) can be reduced to

$$\begin{aligned} \sigma(K^{-2}L^{-n}) &\cong \binom{8}{n} p_L^n(b) [1 - p_L(b)]^{8-n} \\ &\quad \times \int_0^{+\infty} p_K^2(b) 2\pi b db \\ &= \binom{8}{n} p_L^n(b) [1 - p_L(b)]^{8-n} \sigma_{KK}. \end{aligned} \quad (4)$$

In our measurements the $K\alpha_1 L^{-1}$ satellite lines could be observed and resolved from the parent $K\alpha_1$ diagram line. From the $I(K\alpha_1 L^{-1})/I(K\alpha_1)$ yield ratios, the following ionization probabilities p_L were deduced: 0.0034 for Zr, 0.0039 for Mo, and 0.0035 for Pd. It is thus obvious from (4) that for all targets

$$\sigma(K^{-2}L^{-n}) \ll \sigma(K^{-2}L^{-1}) \ll \sigma_{KK}. \quad (5)$$

For these reasons we assumed that in our case $\omega_{KK} \approx \omega_K$. Considering only the most intense transitions, Eq. (2) can be reduced to

$$\frac{\sigma_{KK}}{\sigma_K} = \frac{I(K\alpha_1^h)}{I(K\alpha_1)} \frac{1 + \frac{I(K\alpha_2^h)}{I(K\alpha_1^h)}}{1 + \frac{I(K\alpha_2)}{I(K\alpha_1)}} \frac{1 + \frac{I(K\beta^h)}{I(K\alpha^h)}}{1 + \frac{I(K\beta)}{I(K\alpha)}}. \quad (6)$$

The intensity ratios $I(K\alpha_1^h)/I(K\alpha_1)$, $I(K\alpha_2^h)/I(K\alpha_1^h)$, and $I(K\alpha_2)/I(K\alpha_1)$ were extracted from the experiment and corrected for the different absorption in the target and crystal.

As no $K\beta$ x-ray spectra were observed in the present experiment, the ratios $I(K\beta)/I(K\alpha)$ and $I(K\beta^h)/I(K\alpha^h)$ were calculated using the GRASP code. Results of the latter calculations are given in Table V, those of $(\sigma_{KK}/\sigma_K)_{\text{expt}}$ in Table VI where the values of the different ratios appearing in Eq. (6) are also indi-

cated.

The single and double K -shell ionization cross sections were calculated within the SCA independent-particle approximation with the computer code IONHYD of Trautmann *et al.* [35,36], using hyperbolic classical trajectories and relativistic hydrogenic electronic wave functions. Recoil terms were included. Results are presented in Table VII.

Finally using Eq. (1) and the values of $(\sigma_{KK}/\sigma_K)_{\text{expt}}$ and σ_K^{SCA} listed in Tables VI and VII, respectively, we determined the cross sections $\sigma_{KK}^{\text{expt}}$. Our results are shown in Fig. 8 where one can see that SCA theory, using the independent-particle model, overestimates in a significant way the σ_{KK} cross sections.

A similar conclusion was drawn for lighter element targets (Ca, Ti, V, and Cr) bombarded by 1.3 to 1.7 MeV protons [37]. In this study the observed discrepancies between experiment and standard SCA theory could be partly removed by using different ionization probabilities for the two K electrons. Due to the binding energy increase of the K shell following the removal of the first electron, the second K electron is expected to be ejected with a smaller probability than the first one ($p'_K < p_K$). Replacing p_K^2 by $p_K p'_K$ in the calculation of the double K -shell ionization cross section, i.e., by employing the expression:

$$\sigma'_{KK} = \int_0^{+\infty} p_K(b) p'_K(b) 2\pi b db \quad (7)$$

instead of

$$\sigma_{KK} = \int_0^{+\infty} p_K^2(b) 2\pi b db \quad (8)$$

a much better agreement with experiment was obtained by this group, the σ'_{KK} values being about 20% smaller than the σ_{KK} ones. For increasing atomic number Z one expects the differences between σ_{KK} and σ'_{KK} to decrease. A simple estimation was performed for palladium. The p'_K was deduced by introducing in the SCA calculations the K -electron binding energy in a singly K -shell ionized atom, which was calculated with the GRASP code. Using the obtained value for p'_K in Eq. (7) the calculated σ'_{KK} was finally found to be about 4% smaller than the σ_{KK} given in Table VII. We are, therefore, inclined to attribute also to this effect a part of the discrepancies evinced by our experiment.

TABLE VI. Experimental ratios of double (σ_{KK}) to single (σ_K) K -shell ionization cross sections for ionization by 100 MeV ${}^4\text{He}^{2+}$ ions (4.4(4) [-4] means $(4.4 \pm 0.4) \times 10^{-4}$).

Element	$I(K\alpha_1^h)/I(K\alpha_1)$	$\frac{1 + I(K\alpha_2^h)/I(K\alpha_1^h)}{1 + I(K\alpha_2)/I(K\alpha_1)}$	$\frac{1 + I(K\beta^h)/I(K\alpha^h)}{1 + I(K\beta)/I(K\alpha)}$	$\frac{\sigma_{KK}}{\sigma_K} \text{ expt}$
${}_{40}\text{Zr}$	4.5(4) [-4]	1.13 (8)	1.003	5.1(6) [-4]
${}_{42}\text{Mo}$	4.0(4) [-4]	1.15 (6)	1.007	4.7(5) [-4]
${}_{46}\text{Pd}$	3.5(5) [-4]	1.04 (10)	1.002	3.6(6) [-4]

TABLE VII. Calculated single (σ_K) and double (σ_{KK}) K -shell ionization cross sections in barns for ionization by ${}^4\text{He}^{2+}$ ions of 100 MeV. The calculations were performed within the independent-particle semiclassical approximation (SCA) model. (8.20 [2] means 8.20×10^2).

Element	σ_K	σ_{KK}
${}_{40}\text{Zr}$	8.20 [2]	0.474
${}_{42}\text{Mo}$	6.56 [2]	0.354
${}_{46}\text{Pd}$	4.22 [2]	0.196

It was shown recently that L -shell and especially M -shell ionization probabilities of medium-mass atoms bombarded by charged projectiles were poorly reproduced by SCA calculations using hydrogenic wave functions for the description of the initial and final states of the target atom [38,39]. Replacing the hydrogenic wave functions by relativistic Hartree-Fock wave functions resulted in a much better agreement between theory and experiment [36,40,41]. The K -shell ionization probability, however, is less sensitive to the choice of the wave functions so that no significant change for σ_K and σ_{KK} is expected when using Hartree-Fock wave functions in the SCA calculations.

Atoms having double K -shell vacancies can deexcite radiatively by the following two different mechanisms: (i) $1s^{-2} \rightarrow 1s^{-1}2p^{-1}$ by one-electron-one-photon (OEOP) transition or (ii) $1s^{-2} \rightarrow 2s^{-1}2p^{-1}$ by two-electron-one-photon (TEOP) correlated transitions. The first mechanism corresponds to the K -hypersatellite transitions. The second one was predicted by Heisenberg [42] already in 1925 but the first observation of TEOP transitions took place only in 1975 in a heavy-ion collision experiment [43]. Since then these transitions have been observed in a variety of experiments in which the double K -shell ionization was produced by impact with

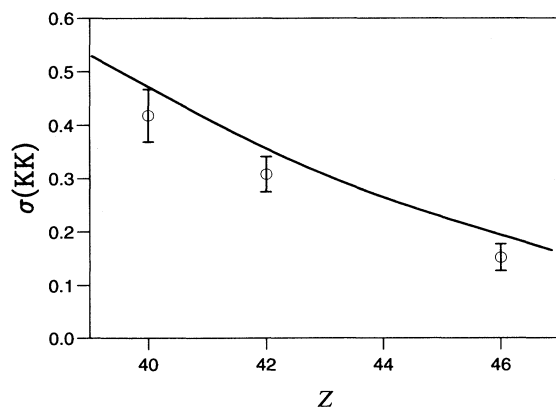


FIG. 8. Double K -shell ionization cross sections σ_{KK} in barns deduced from the present experiment. The curve represents the results of SCA calculations within the independent-particle model.

heavy-ions, electron-capture decay, as well as proton- and electron-induced excitations [44, and references therein]. Available experimental data concerning the branching ratio $B = I(\text{TEOP})/I(\text{OEOP})$ are, however, still scarce and sometimes inconsistent. For aluminium, Auerhammer *et al.* [44] found for instance a branching ratio $B(\text{Al}) = (2.2 \pm 0.8) \times 10^{-3}$ while Salem *et al.* [45] obtained for several first transition series elements the following results: $B(\text{Cr}) = 0.88 \pm 0.44$, $B(\text{Fe}) = 0.48 \pm 0.22$, $B(\text{Co}) = 0.51 \pm 0.20$, and $B(\text{Cu}) = 0.73 \pm 0.40$. Several models were proposed to explain the TEOP mechanism. Most of these calculations predict a nonvanishing branching ratio. Åberg *et al.* [46] found for B the following simple result:

$$B = (E_2/E_1)^3 [D_0(1s2s)]^2, \quad (9)$$

where E_1 is the average hypersatellite transition energy, E_2 the average two-electron-one-photon transition energy, and $D_0(1s2s)$ the $1s2s$ radial overlap integral which is approximatively given by $0.187/Z$.

Using Eq. (9) we find a theoretical value of 1.6×10^{-3} for Al, in good agreement with the experimental result of Auerhammer *et al.*, and an average value of 3.6×10^{-4} for the first transition series elements, which is about 2000 times smaller than the average value of 0.65 obtained by Salem *et al.* However, since Salem's results have not to our knowledge been confirmed by any other experiment, we are inclined to trust the theoretical predictions and, as a consequence, to neglect the TEOP strength, which should be in our case about 5000 times smaller than the OEOP one.

A double K -shell vacancy may result from a shake process following a single K -shell ionization provided that the ejected K electron has a kinetic energy higher than the binding energy B_K of the K shell. In collisions of 100 MeV ${}^4\text{He}^{2+}$ ions with targets of Zr ($B_K \cong 18.0$ keV), Mo ($B_K \cong 20.0$ keV), and Pd ($B_K \cong 24.4$ keV), δ electrons are ejected from the K shell with maximum energies of about 46, 48, and 53 keV, respectively. The contribution of shake effects, which are not included in the SCA theory, to the observed K hypersatellite yields cannot, therefore, be excluded *a priori*. Calculations based on the sudden approximation model and performed for elements from $Z = 2$ to $Z = 36$ [47] give for the heaviest element a probability of 2×10^{-5} for electron shake from the K shell as a result of $1s$ vacancy production. Since shake probabilities decrease with Z , one could expect that the contribution of shake effects to the hypersatellite yields observed in our experiment do not exceed 4% (see Table VI). Predictions of shake probabilities following the sudden approximation method, however, are only reliable when the double ionization concerns different subshells. When considering double ionization in the same subshell, one can no more simply assume that the orbitals relax independently of one another and one has to take into account correlation effects [5]. The most general and powerful method to describe such correlation effects is the many-body perturbation theory. This method is however very difficult and, to our knowledge, no calculation has yet been carried out in the case of double K -shell ionization of a many-electron atom.

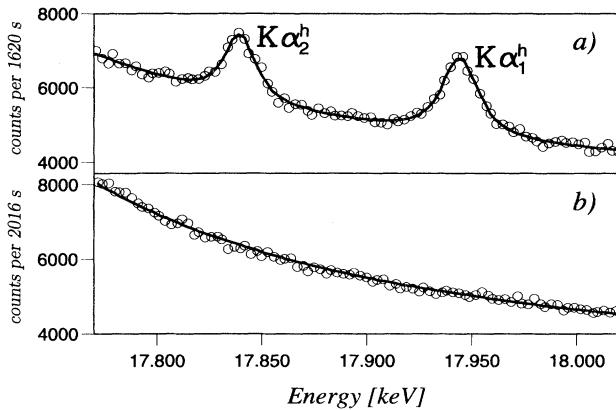


FIG. 9. X-ray spectra of molybdenum in the region of $K\alpha$ hypersatellites resulting from (a) 100 MeV ${}^4\text{He}^{2+}$ bombardment, (b) photoionization (x-ray tube with a Au anode operated at 80 kV and 30 mA). The probability for a K -shell shakeoff process following a K -shell photoionization is extremely small for medium-mass atoms. This is confirmed by the spectrum (b) where no hypersatellites could be observed.

For this reason a complementary measurement of the photoinduced $K\alpha$ hypersatellite spectrum of molybdenum was performed in order to determine directly the shake contribution to the double K -shell ionization observed in the He experiment. The spectrum was measured by means of a similar spectrometer installed at the University of Fribourg and equipped with a 100 kV Au x-ray tube [15]. No hypersatellite structure was observed in this spectrum [see Fig. 9(b)]. From the analysis an upper limit of 5×10^{-5} was deduced for the $I(K\alpha^h)/I(K\alpha)$

yield ratio. Hence no corrections were performed on the hypersatellite yields of the He experiment.

V. CONCLUSION

High precision measurements of the radiative decay $K^{-2} \rightarrow K^{-1}L^{-1}$ of doubly K -shell ionized atoms of zirconium, molybdenum, and palladium induced by 100 MeV ${}^4\text{He}^{2+}$ were performed. The so-called hypersatellite transitions were observed with a transmission crystal spectrometer of modified DuMond slit geometry. Satisfactory agreement with DHS calculations and with MCDF calculations (both including Breit interaction) was found for the energies, whereas for the intensity ratios of the hypersatellites the theoretical predictions underestimate the experimental results. The observed natural linewidths of the hypersatellites could be well reproduced by a crude semiempirical model. The double K -shell ionization cross sections deduced from the relative yields of the hypersatellites were found to be smaller than the results of theoretical independent particle SCA predictions. Possible causes for the observed discrepancies such as, for instance, the use of equal ionization probabilities for the two K electrons or the nonconsideration of the competitive TEOP transitions were discussed.

ACKNOWLEDGMENTS

This work was supported in part by the Swiss National Science Foundation and by the Paul Scherrer Institute (PSI). We thank Dr. Stambach and Dr. Schmelzbach and the cyclotron crew for very good beam conditions. Partial financial support for this work was provided by the Polish Committee for Scientific Research (KBN) (Grant Nos. 2 p302 119 07 and 2 2322 92 03).

- [1] B. Perny *et al.*, *Phys. Rev. A* **36**, 2120 (1987).
- [2] M.W. Carlen *et al.*, *Z. Phys. D* **23**, 71 (1992).
- [3] J.P. Briand *et al.*, *Phys. Lett. A* **49**, 51 (1974).
- [4] C.W.E. van Eijk, J. Wijnhorst, and M.A. Popelier, *Phys. Rev. A* **20**, 1749 (1979).
- [5] J.P. Briand *et al.*, *Phys. Rev. A* **23**, 39 (1981).
- [6] O. Keski-Rahkonen, J. Saijonmaa, M. Suvanen, and A. Servomaa, *Phys. Scr.* **16**, 105 (1977).
- [7] J. Ahopelto, E. Rantavuori, and O. Keski-Rahkonen, *Phys. Scr.* **20**, 71 (1979).
- [8] J. Saijonmaa, *Phys. Scr.* **17**, 4576 (1978).
- [9] E. Mikkola, O. Keski-Rahkonen, and R. Kuoppala, *Phys. Scr.* **19**, 29 (1979).
- [10] P. Richard, W. Hodge, and C.F. Moore, *Phys. Rev. Lett.* **29**, 393 (1972).
- [11] P. Richard, D.K. Olsen, R. Kauffman, and C.F. Moore, *Phys. Rev. A* **7**, 1437 (1973).
- [12] R.L. Watson, J.R. White, and F.E. Jenson, *Phys. Lett. A* **67**, 269 (1978).
- [13] O. Benka, R.L. Watson, and B. Bandong, *Phys. Rev. A* **28**, 3334 (1983).
- [14] B. Perny *et al.*, *Nucl. Instrum. Methods Phys. Res. Sect. A* **267**, 120 (1988).
- [15] J. Hozzowska, J.-Cl. Dousse, and Ch. Rhême, *Phys. Rev. A* **50**, 123 (1994).
- [16] B. Boschung (unpublished).
- [17] B. Jeckelmann *et al.*, *Nucl. Instrum. Methods Phys. Res. Sect. A* **241**, 191 (1985).
- [18] J.A. Bearden and A.F. Burr, *Rev. Mod. Phys.* **39**, 78 (1967).
- [19] F. James and M. Roos, *Comp. Phys. Comm.* **10**, 343 (1975).
- [20] K.W. Hill, B.L. Doyle, S.M. Shafroth, D.H. Madison, and R.D. Deslattes, *Phys. Rev. A* **13**, 1334 (1976).
- [21] L.M. Watson, R.K. Dimond, and D.J. Fabian, in *Soft X-Ray Band Spectra*, edited by D.J. Fabian (Academic Press, New York, 1968), pp. 45–58.
- [22] C. Senemaud and M.T. Costa Lima, *Phys. Lett. A* **47**, 395 (1974).
- [23] K. Tsutsumi and H. Nakamori, *J. Phys. Soc. Jpn.* **25**, 1419 (1986).
- [24] M.H. Chen, B. Crasemann, and H. Mark, *Phys. Rev. A* **25**, 391 (1982).
- [25] I.P. Grant *et al.*, *Comput. Phys. Commun.* **21**, 207 (1980).

- [26] K.G. Dyllal *et al.*, *Comput. Phys. Commun.* **55**, 425 (1989).
- [27] M. Polasik, *Phys. Rev. A* **40**, 4361 (1989).
- [28] J.P. Mossé, P. Chevallier, and J.P. Briand, *Z. Phys. A* **322**, 207 (1985).
- [29] M.O. Krause and J.H. Oliver, *J. Phys. Chem. Ref. Data* **8**, 307 (1979).
- [30] T. Åberg *et al.*, *J. Phys. B* **9**, 2815 (1976).
- [31] J.P. Briand *et al.*, *Phys. Fenn.* **9**, 409 (1974).
- [32] J.P. Briand, P. Chevallier, M. Tavernier, and J.P. Rozet, *Phys. Rev. Lett.* **27**, 777 (1974).
- [33] C.P. Bhalla and M. Hein, *Phys. Rev. Lett.* **30**, 39 (1973).
- [34] C.P. Bhalla, *J. Phys. B* **8**, 2787 (1975).
- [35] D. Trautmann and F. Rösel, *Nucl. Instrum. Methods* **169**, 259 (1980).
- [36] Z. Halabuka, W.F. Perger, and D. Trautmann, *Z. Phys. D* **29**, 151 (1994).
- [37] V. Cindro *et al.*, *J. Phys. B* **22**, 2161 (1989).
- [38] P. Rymuza *et al.*, *Z. Phys. D* **23**, 81 (1992).
- [39] M.W. Carlen *et al.*, *Phys. Rev. A* **46**, 3893 (1992).
- [40] W.F. Perger, Z. Halabuka, and D. Trautmann, *Comp. Phys. Comm.* **76**, 250 (1993).
- [41] M.W. Carlen *et al.*, *Phys. Rev. A* **49**, 2524 (1994).
- [42] W. Heisenberg, *Z. Phys.* **32**, 841 (1925).
- [43] W. Wölfl *et al.*, *Phys. Rev. Lett.* **35**, 656 (1975).
- [44] J. Auerhammer, H. Genz, A. Kumar, and A. Richter, *Phys. Rev. A* **38**, 688 (1988).
- [45] S.I. Salem, A. Kumar, and B.L. Scott, *Phys. Rev. A* **29**, 2634 (1984).
- [46] T. Åberg, K.A. Jamison, and P. Richard, *Phys. Rev. Lett.* **37**, 63 (1976).
- [47] T. Mukoyama and K. Taniguchi, *Phys. Rev. A* **36**, 693 (1987).
- [48] K. Ilakovac, M. Vesković, V. Horvat, and S. Kaučić, *Phys. Rev. A* **42**, 3984 (1990).
- [49] Y. Isozumi *et al.*, *Phys. Rev. C* **28**, 3070 (1982).
- [50] N. Cue, W. Scholz, and A. Li-Scholz, *Phys. Lett. A* **63**, 54 (1977).
- [51] V. Horvat and K. Ilakovac, *Phys. Rev. A* **31**, 1543 (1985).
- [52] S.I. Salem, *Phys. Rev. A* **21**, 858 (1980).